JOURNAL OF MATERIALS SCIENCE **39** (2004) 3497– 3500

Surface integrity effects on turned 6061 and 6061-T6 aluminum alloys

C. K. TOH*, S. KANNO
Singapore Institute of Manufacturing Technology (SIMTech), Machining Technology Group, 71 Nanyang Drive, Singapore 638075, Singapore
E-mail: cktoh@SIMTech.a-star.edu.sg

Aluminum alloys have been the most widely used structural materials in the aerospace and automotive industries for several decades. Currently, one of the most commonly used aluminum alloys is the 6000-series (Al-Mg-Si). The 6000-series alloys have much better corrosion resistance. By further applying a T6 heat treatment, the toughness and resistance to fatigue crack growth can be improved, typically increasing its strength by as much as 30% [1]. This attributes to superior mechanical properties such as a high strength/weight ratio, good corrosion resistance, weldability, and deformability [2].

Surface integrity is defined as the intrinsic or enhanced condition of a surface produced by a machining process [3]. The functional behavior and dimensional stability of a finished component is greatly influenced by the surface integrity induced during machining. To gain a better understanding of the effects of process parameters on the machined surface, basic knowledge such as surface integrity analysis will lead to the generation of counteractive machining procedures to improve component fatigue life and machinability.

While there appears to be appreciable amounts of research on the surface integrity of ferrous alloys, notably hardened steels [4–6], there do not seem to be any literature reports on systematic studies of surface integrity of non-ferrous alloys such as turned aluminum alloys. This letter is concerned with the surface integrity analysis

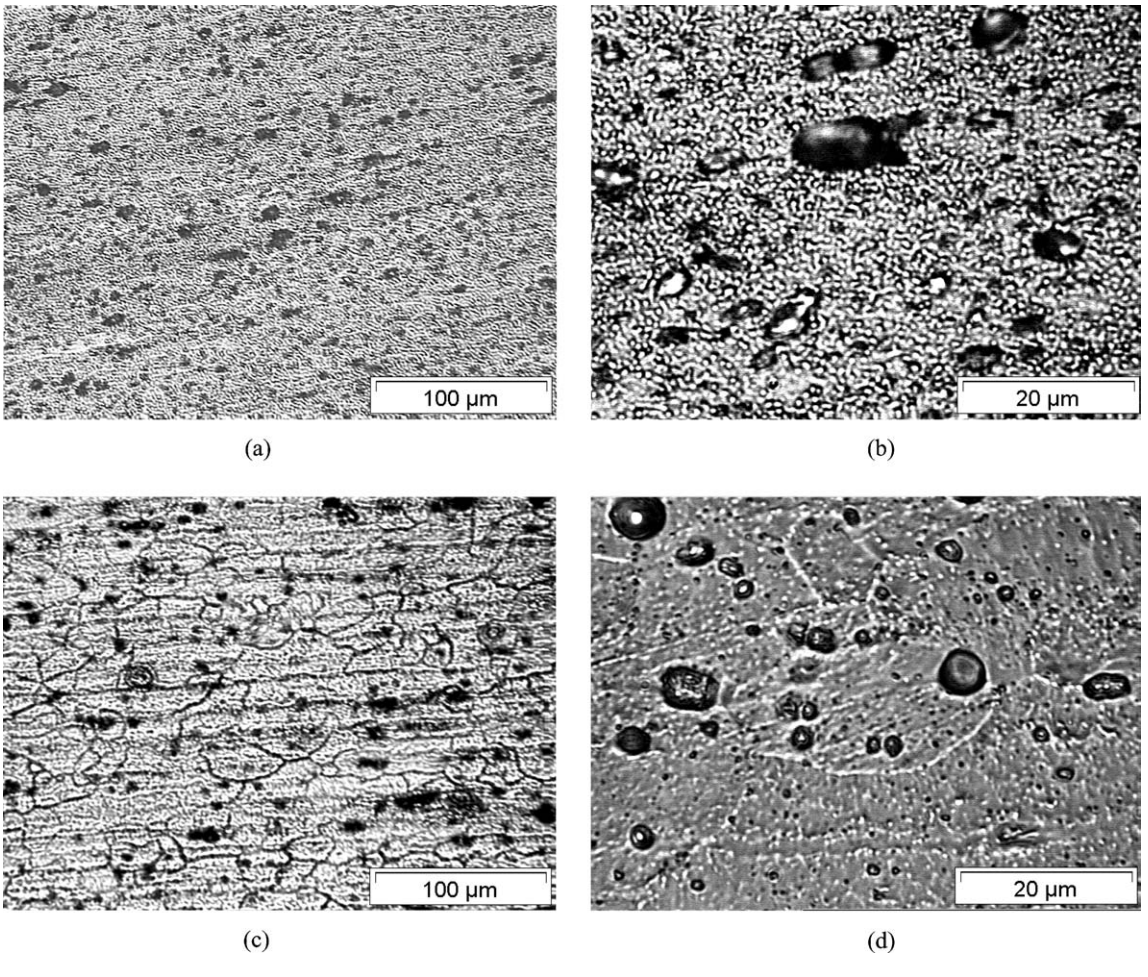

Figure 1 Typical optical micrographs depicting the bulk microstructure of the aluminum alloy: (a) 6061 at ×200 magnification, (b) 6061 at ×1000 magnification, (c) 6061-T6 at ×200 magnification and (d) 6061-T6 at ×1000 magnification.

*Author to whom all correspondence should be addressed.

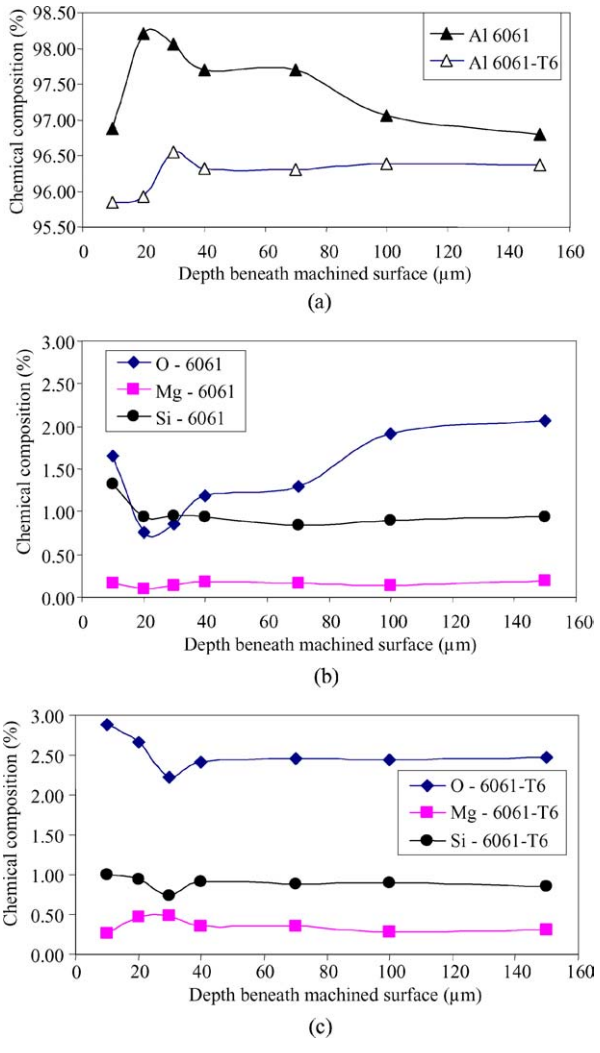

Figure 2 Composition profiles of aluminum alloy measured from the machined surface along the depth for: (a) contents Al for 6061 and 6061-T6, contents of O, Mg and Si for, (b) 6061 and (c) 6061-T6.

on machined 6061 and 6061-T6 aluminum alloys produced by finish turning. The roles of microstructure, microhardness, and residual stress analysis beneath the machined surfaces are investigated and reported in order to shed some light on its surface integrity analysis.

Aluminum alloy 6061 with a nominal composition of 0.4% Si, 0.7% Fe, 0.15% Cu, 0.15% Mn, 0.8% Mg, 0.04% Cr, 0.25% Zn, 0.15% Ti and balance Al was used for two different processes to be investigated and compared. The processing stage was split into two phases: the untreated and the treated phase. T6 heat treatment was implemented for the treated phase. Both materials were die-casted into a pre-deformed shape followed by a cold forging process to form a final desired shape. The final deformed shape was finish turned on a double turret NC Lathe with a maximum spindle speed of 3000 rpm. Polycrystalline diamond (PCD) cutting tools attached on an insert with a top rake angle of 8° were used. Turning was performed at a spindle speed of 3000 rpm, feed per revolution of 0.3 mm/rev, and a depth cut of 0.3 mm. Flood coolant oil with 5% emulsion was employed throughout the machining tests.

Microhardness measurements were undertaken with a Vickers indenter using a load of 10 g and a loading time of 15 s. Five indentation loads were carried out on the middle of the sample to obtain the baseline value of the bulk microhardness. This was to ensure that the variation of the microhardness did not vary by more than 10% due to work hardening effect. A series of three readings were taken at equispaced distances at approximately predefined nominal depths measured from the surface. In this way, microhardness sensitivity due to hard particles can be averaged out to obtain more accurate readings. Measurements were halted once the bulk microhardness of the specimens was obtained.

The residual stress measurements were performed across the feed directions of the turned surface using a goniometer with a position sensitive detector (PSD). The X-ray radiation source used was Cu K_α. The diffraction angle 2θ employed for detecting peak aluminum was 138° and 10 PSI angles from —20° to 25° were used. The Poisson's ratio employed in this analysis was 0.32. The measurements were performed using a collimator size of 0.5 mm. Before carrying out any subsurface measurements, the machined surface intended for polishing was masked exposing an area of approximately 5 mm × 5 mm. The surface was then electrochemically polished by dissolution of the material

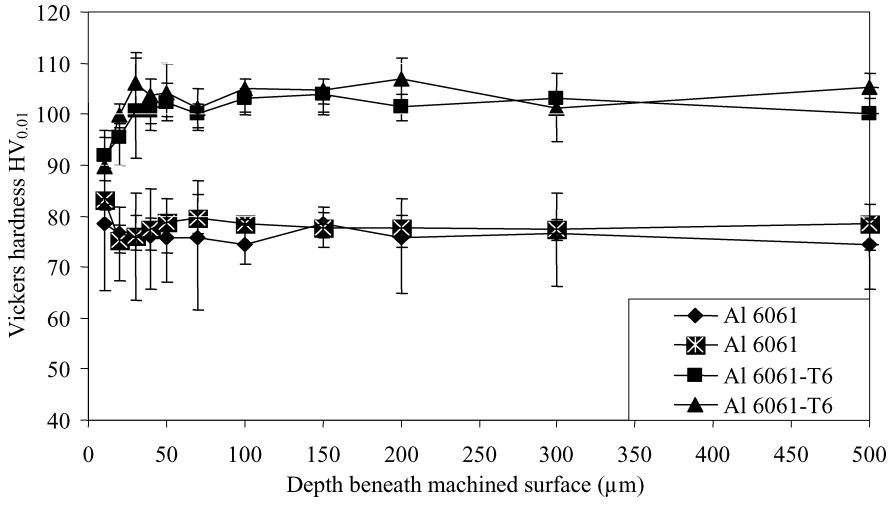

Figure 3 Microhardness profiles measured from the machined surface along the depth for aluminum 6061 and 6061-T6 alloys. Measurements were replicated twice on different samples to ascertain the results. The range bars indicate maximum and minimum values.

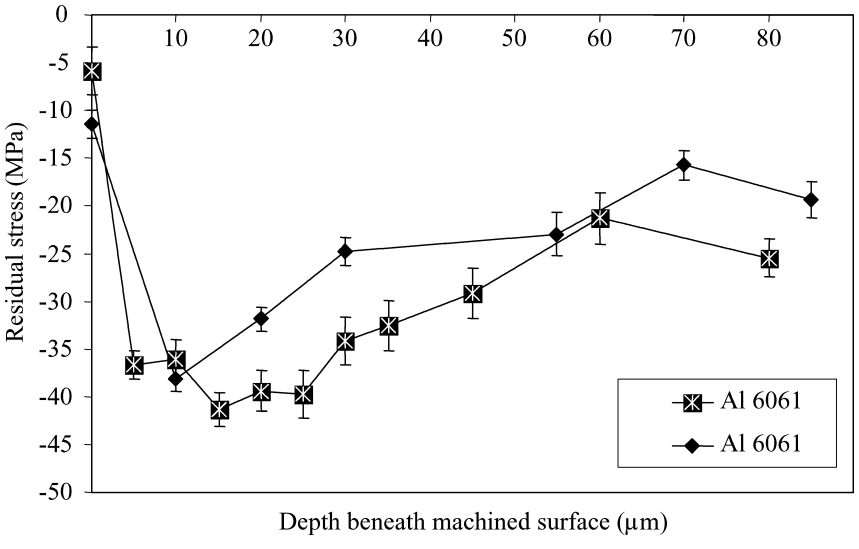

(a)

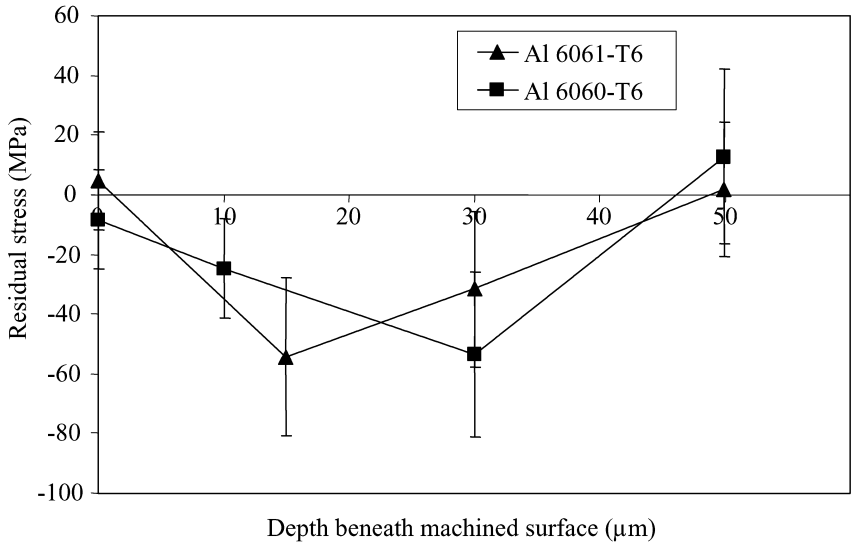

(b)

Figure 4 Residual stress profiles measured from the machined surface along the depth for aluminum: (a) 6061 and (b) 6061-T6 alloys. Measurements were replicated twice on different samples to ascertain the results. The range bars indicate maximum and minimum values.

using a classified "B" type etchant provided by Rigaku Corporation. The etched sample was measured using a micrometer.

Fig. 1 shows the typical optical bulk microstructure of Al 6061 and Al 6061-T6 alloys. Comparing Fig. 1a and c, and 1b and d respectively at higher magnification, shows that 6061-T6 exhibits much larger recrystallized grains characterized by their distinct boundaries. The presence of impur elements, typified by their dark constituents, is believed to be impurities formed during the casting process. The presence of impur elements, such as iron and silicon, in the alloy results in the precipitation of a high volume fraction of coarse insoluble iron-rich and silicon-rich constituents during casting [8].

To realize an in-depth understanding of any composition changes that occur along the depth of the specimens, chemical composition of the main elements was analyzed and plotted along the depth beneath the machined surfaces, see Fig. 2. For 6061 alloy, it is interesting to note that there is a moderate drop in chemical contents of O, Mg, and Si at the 20-μm depth, coupled with a relatively drastic increase in Al content beneath the machined surface. Similar observations on the distribution of various elements are also made for 6061-T6 sample, albeit with a moderate increase in Mg content at the depth of 30 μm. A plausible explanation for the decrease in chemical contents in the depths is the decrease in the void volume fraction due to the applied load that results from stresses acting on the machined surface during the turning process, due to the increase in the applied load/displacement. With the occurrence of compression, fracture sites beneath the machined surface start to inhibit and that facilitates inhibitation of the nucleation and growth of voids around the grain boundaries and undissolved iron-rich and silicon-rich intermetallics. The increase in Mg content for 6061-T6 sample suggests the presence of insoluble magnesium-rich constituent phase.

Fig. 3 plots the microhardness variation curves with respect to the depth measured beneath the machined surface. Analysis of the microhardness depth profiles on 6061 samples shows an increase in microhardness values ranging from 15 to 20 $HV_{0.01}$ confining to a depth of

around 20 μm from the machined surface. In contrast, the microhardness depth profiles on 6061-T6 samples display a decrease in microhardness values of about 20 $HV_{0.01}$ confining to a depth of around 30 μm from the machined surface before reaching its stable bulk microhardness values. Under same cutting conditions, the higher thermal conductivity (180 W/mK) of 6061 will result in a higher cutting temperature to be conducted into the workpiece and consequently a higher flow stress is resulted due to its lower shear strength (80 MPa). This in turn leads to an increase in surface deformation that ultimately leads to an increase in the work hardening of the machined surface dominated by plastic deformation. On the other hand, for 6061-T6 samples, thermal softening effect prevails in that the lower thermal conductivity (160 W/mK) accentuates a lower heat input into the material surface, coupled with a higher shear strength (205 MPa), which will eventually result in a lower shear stress input. Hence elastic deformation without exceeding its yield strength contributes to its thermal softening effect. The higher bulk microhardness of 6061-T6 samples is due to a precipitation hardening process in which the presence of Si inhibits recrystallization [7, 8].

Fig. 4 depicts the residual stress distributions measured on and beneath the machined surfaces for both aluminum alloys. In general, compressive residual stress regimes are observed for both material samples. It has been well documented that compressive residual stress dominated by mechanical effects inhibits crack growth and subsequently enhances surface properties and interfacial strength [9, 10]. Significantly, 6061 compressive residual stress regimes extend deeper into the depth with relatively lower compressive stress magnitudes. Furthermore, 6061 compressive residual stress magnitudes peak at depths measured between 10 and 15 μm, about 5 to 15 μm lesser for 6061-T6 samples. Notice that the depths locating the maximum compressive residual stress magnitudes coincide with that of the chemical content profiles of the respective aluminum alloy samples, see Fig. 4. Therefore, it can be inferred that the maximum compressive stresses are induced by maximum principal stresses that result in a decrease in the void volume fraction via inhibitation of void growth and coalescence. The high-range values on 6061-T6 samples shown in Fig. 4b are attributed to their coarse and large grain sizes that deliver a huge contribution to their diffraction peak.

Acknowledgments

The work originated from an industrial SIMTech project code I02-T-218. Thanks are due to Mr. Wilson Sim Mong Chye, Mr. Jeffrey Goh, Mr. Shaw Kah Chuan, Ms. Ng Fern Lan, and Dr. Andrew Spowage for their helpful advice and technical support.

References

1. J. P. IMMARIGEON, R. T. HOLT, A. K. KOUL, L. ZHAO, W. WALLACE and J. C. BEDDOES, *Mater. Character.* **35** (1995) 41.
2. W. S. LEE, J. C. SHYU and S. T. CHIOU, *Scr. Mater.* **42** (2000) 51.
3. M. FIELD and J. F. KAHLES, *CIRP ANNALS* **21** (1971) 153.
4. J. RECH and A. MOISAN, *Int. J. Mach. Tools Manuf.* **43** (2003) 543.
5. M. JACOBSON, *Proc. Inst. Mech. Eng. Part B-J. Eng. Manuf.* **216** (2002) 47.
6. A. M. ABRAO and D. K. ASPINWALL, *Wear* **196** (1996) 279.
7. A. HEINZ, A. HESZLER, C. KEIDEL, S. MOLDENHAUER, R. BENEDICTUS and W. S. MILLER, *Mater. Sci. Eng. A-Struct. Meter. Prop. Microstruct. Process.* **280** (2000) 102.
8. P. C. LAM, T. S. SRIVATSAN, B. HOTTON and M. AL-HAJRI, *Mater. Lett.* **45** (2000) 186.
9. P. KADOLKAR and N. B. DAHOTRE, *Mater. Sci. Eng.* **342** (2003) 183.
10. Y. MATSUMOTO, M. M. BARASH and C. R. LIU, *J. Eng. Ind. Trans. ASME.* **108** (1986) 169.

Received 4 December 2003
and accepted 21 January 2004